Theor Appl Climatol
DOI 10.1007/s00704-011-0504-y

ORIGINAL PAPER

Effects of convective scale downdrafts on the rainfall simulation in NCAR-CAM3

Sandeep Sahany · Saroj K. Mishra

Received: 16 December 2010 / Accepted: 4 August 2011

Abstract In this work, an attempt is made to systematically evaluate the effect of convective scale downdrafts on the model-simulated rainfall, in both aqua- and actual-planet frameworks, using the NCAR CAM3. From the aqua-planet simulations, it was found that there is a reduction in the total rainfall (TRF) with increase in the intensity of downdrafts, which is primarily attributed to the reduction in the deep convective component (DRF). However, with stronger downdrafts, the shallow convective and the large-scale components (SRF and LRF, respectively) are found to increase. The reduction in DRF is due to the increased evaporation of convective precipitation within the downdrafts. It is found that, with intense downdrafts, there is an increase in relative humidity throughout the troposphere, due to the combined effect of both moisture and temperature. There is an overall increase in specific humidity of the atmosphere with stronger downdrafts, excepting at around the 900-hPa level. In addition, there is a reduction in temperature throughout the troposphere, primarily due to the reduction in the overall temperature tendency due to moist processes and that due to the radiative processes. The changes in the radiative forcing are found to be primarily due to a significant increase in the low cloud fraction with strong downdrafts. In the actual-planet framework, it is seen that, with strong convective downdrafts, there is a reduction in TRF and DRF and a corresponding increase in SRF and LRF, similar to the results obtained from the aqua-planet simulations. The vertical structures of the thermodynamic variables (RH, q, and T) show similar sensitivity to the downdraft intensity as that seen in the aqua-planet framework. Sensitivity of frequency and intensity of model-simulated rainfall to the downdraft intensity was also analyzed, and it was seen that there were significant differences in the frequency distribution of rainfall. It was seen that, with an increase in downdraft intensity, there is an increase in the frequency of light rain (1–10 mm/day) for TRF with a corresponding reduction in all other rainfall bins. A similar behavior was seen for the DRF as well, while the SRF and LRF components showed an increase in rainfall accumulation in all the bins. In addition, the impact of convective downdrafts on the mean spatial pattern of rainfall is also analyzed, for the DJF and JJA periods (boreal winter and summer, respectively). For the DJF period, with strong downdrafts, it was seen that grossly over the whole domain, there were a reduction in DRF and an increase in SRF and LRF. In contrast, during JJA, although a major part of the domain showed a reduction in DRF, there were regions like western Arabian Sea and the Somali coast with increase in DRF with intense downdrafts. The SRF and LRF components, however, show a spatially homogeneous increase over almost the entire domain with increase in downdraft intensity.

S. Sahany
Department of Atmospheric and Oceanic Sciences,
University of California, Los Angeles,
Los Angeles, CA, USA

S. K. Mishra (✉)
Institute for Mathematics Applied to Geosciences (IMAGe),
National Center for Atmospheric Research (NCAR),
1850, Table Mesa Drive,
Boulder, CO 80305, USA
e-mail: saroj@ucar.edu

S. K. Mishra
Department of Computer Science, University of Colorado,
Boulder, CO, USA

1 Introduction

Precipitation is considered to be one of the most important outputs of a numerical model, and an overwhelming

Published online: 22 August 2011

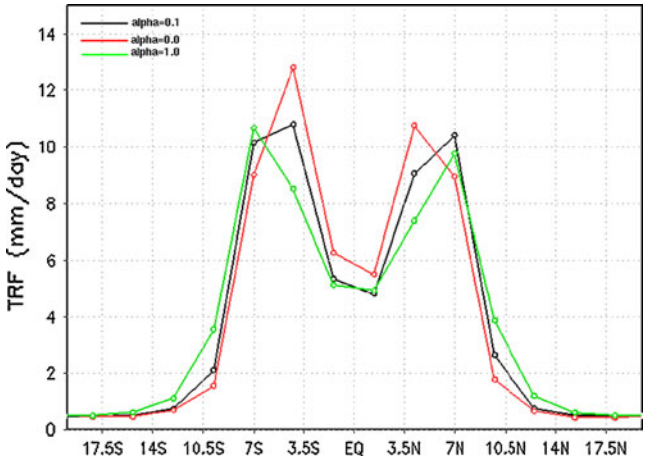

Fig. 1 Zonally averaged time mean total rainfall (TRF) with three different alpha values of 0.0, 0.1 (control), and 1.0

fraction of the modeling community focus their efforts in improving its simulation on various spatio-temporal scales. In most state-of-the-science climate models, total precipitation is the sum of its three components, namely, deep convective, shallow convective, and stratiform rainfall. Each of these components is generally computed by individual parameterization schemes in the model. Among the three aforementioned components of rainfall, the deep convective component forms a major fraction of the total rainfall and plays a significant role in the general circulation of the atmosphere.

Given the fact that deep convective rainfall forms the most important component of the hydrological cycle, it is of considerable interest to realistically simulate this variable in numerical models. The cumulus parameterization scheme that computes the deep convective rainfall in the model has a cloud model at its core, and it essentially consists of an

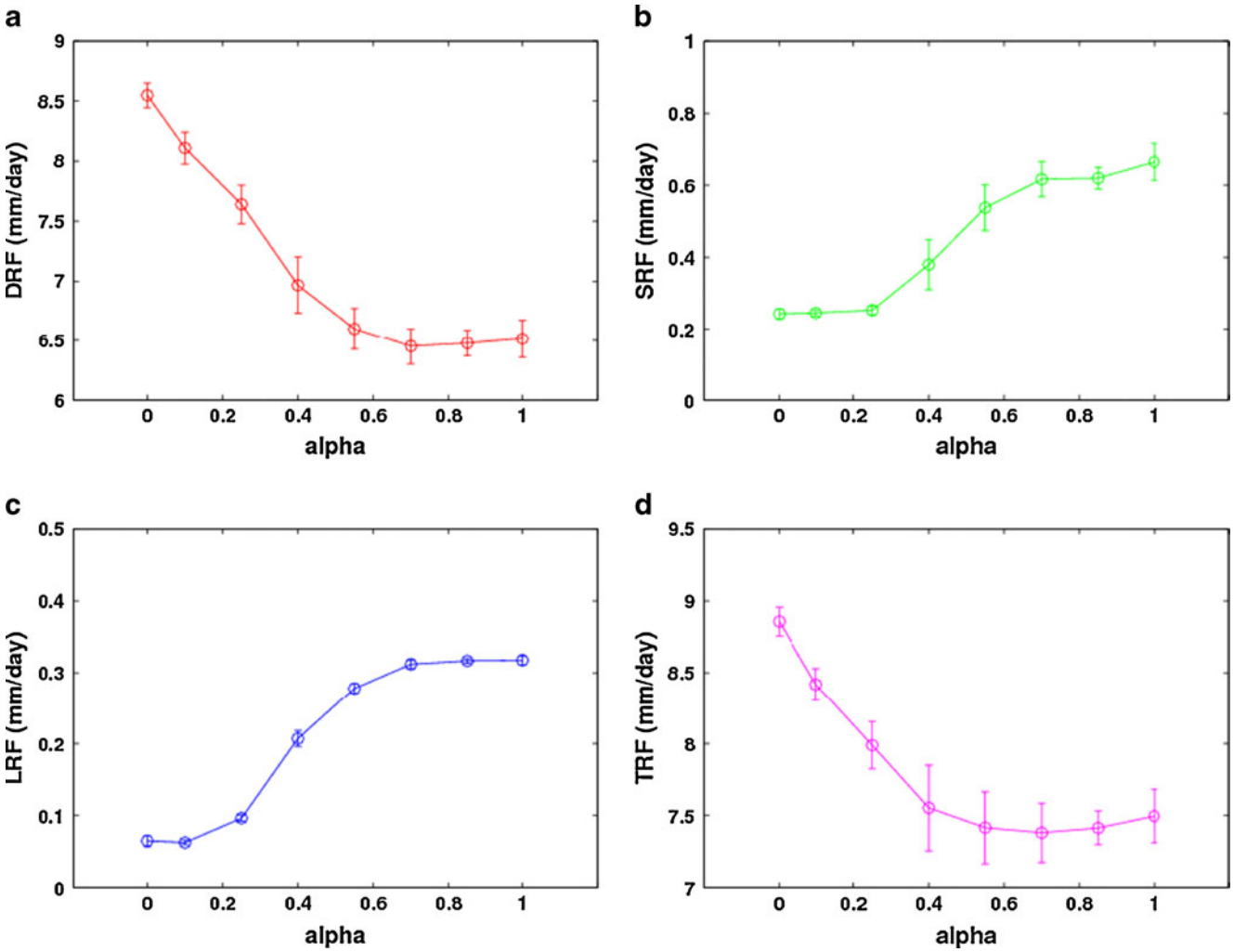

Fig. 2 Area averaged, time mean values of **a** DRF, **b** SRF, **c** LRF, and **d** TRF (mm/day) versus alpha for the region (0E to 360E and 7S to 7N). The *error bars* show the respective standard deviation in time about the time mean values. *TRF* Total rainfall, *DRF* deep convective rainfall, *SRF* shallow convective rainfall, *LRF* large-scale rainfall (also called as stratiform rainfall)

updraft and a downdraft model. In this paper, our primary focus is on the convective downdraft model used in the Zhang McFarlane (1995; hereafter ZM95) convection scheme used in the National Center for Atmospheric Research (NCAR) Community Atmosphere Model version 3 (CAM3).

In ZM95, the authors have carried out an extensive analysis on the performance of the scheme and its sensitivity to different parameters in a single column model (SCM) framework as well as in a three dimensional GCM, using the Canadian Climate Center General Circulation Model (CCC GCM). They clearly showed that model simulations are sensitive to the strength of convective downdrafts. Their SCM results show that downdrafts tend to reduce the mean CAPE in the atmosphere. Based on the above results, they concluded that strong downdrafts provide a powerful mechanism for stabilizing the atmospheric column. Molinari and Corsetti (1985), using the Kuo scheme, showed that the inclusion of downdrafts increases the rate of stabilization of the atmosphere. In a recent study, Sahany and Nanjundiah (2008) (hereafter SN08) investigated the role of convective downdrafts on model simulations in an aqua-planet framework using NCAR CAM3. They showed that, although the rate of CAPE consumption increases with the incorporation of downdrafts, the generation of CAPE increases at an even higher rate, which in turn leads to a more unstable atmosphere.

Although there have been studies in the past highlighting the importance of convective downdrafts in model simu-

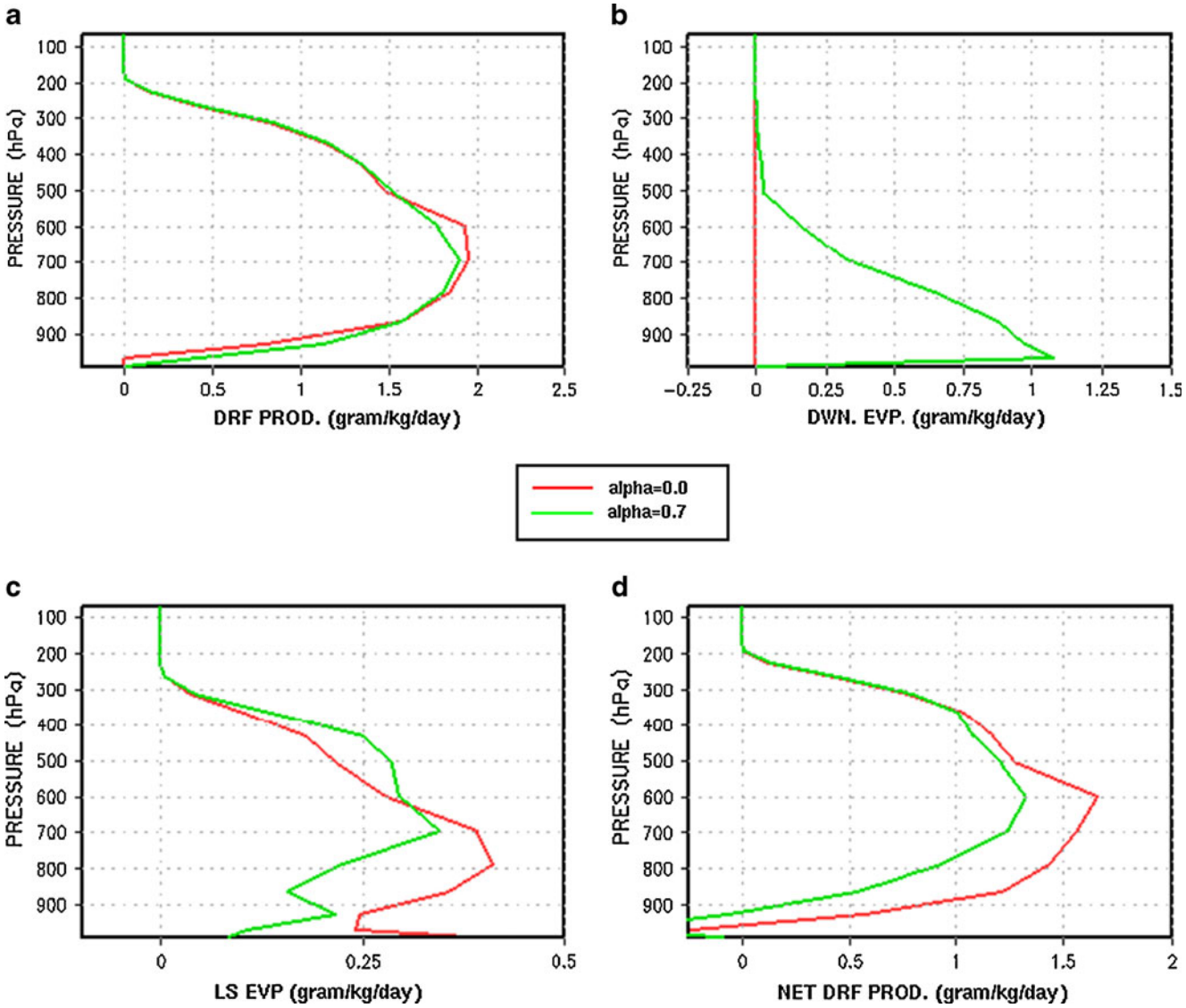

Fig. 3 Vertical profile of the area averaged (0E to 360E and 7S to 7N), time mean, quantities for alpha=0.0 and alpha=0.7: **a** deep convective precipitation production rate (g kg^{-1} day^{-1}), **b** evaporation of the deep convective precipitation within the downdrafts (g kg^{-1} day^{-1}), **c** grid-scale evaporation of the deep convective precipitation (g kg^{-1} day^{-1}), and **d** net deep convective precipitation production rate (g kg^{-1} day^{-1})

lations, none of them present a detailed systematic analysis of the role played by convective downdrafts in rainfall simulation. Convective scale downdrafts are known to modify the vertical structure of temperature and humidity in the atmosphere, with the most direct effect in the boundary layer and the lower free troposphere. This change in the vertical structure of the atmosphere can have significant effects on deep convection and its associated rainfall.

In SN08, the simulations were carried out in an idealized framework and the focus was on deep convective rainfall. So far, its effects on the other two components of rainfall are not known. Secondly, it is desirable to understand its effects in a real planet framework with actual land-ocean-orography distributions and temporally varying boundary conditions. These motivate the current study, and hence, herein we will address the above-mentioned issues.

In Section 2, we discuss the model details, followed by the simulation details in Section 3. The impact of convective downdrafts on model-simulated rainfall and its associated variables is addressed in Section 4. Finally, in Section 5, we summarize the important conclusions from this study.

2 Model details

The numerical model used in this study is CAM3, an atmospheric general circulation model (AGCM) developed

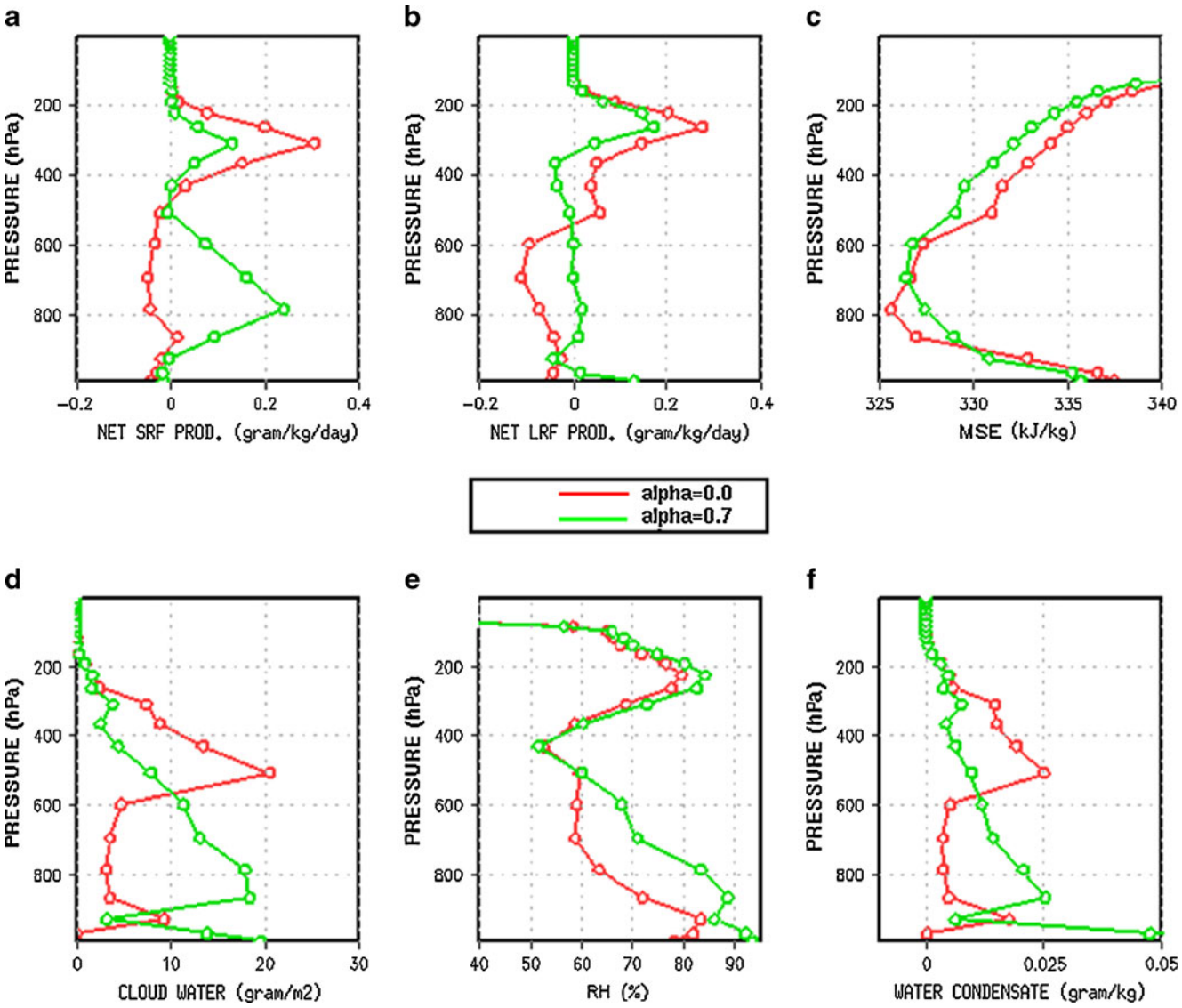

Fig. 4 Vertical profile of the area averaged (0E to 360E and 7S to 7N), time mean, quantities for alpha=0.0 and alpha=0.7: **a** net shallow convective precipitation production rate (g kg^{-1} day^{-1}), **b** net large scale precipitation production rate (g kg^{-1} day^{-1}), **c** moist static energy (kJ/kg), **d** cloud water (g/m^2), **e** relative humidity (%), and **f** water condensate (g/kg)

by NCAR in collaboration with the atmospheric modeling community. The source code, documentation, and input datasets for the model were obtained from the CAM website, i.e., http://www.ccsm.ucar.edu/models/atm-cam.

For this study, the semi-Lagrangian dynamical core was used at 64×128 horizontal resolution with 26 vertical levels. The model uses a hybrid vertical coordinate, which is terrain following at earth's surface, but reduces to pressure coordinate at higher levels near the tropopause.

The physical parameterization package consists of moist precipitation processes, clouds and radiation processes, surface processes, and turbulent mixing processes. The moist precipitation processes consist of deep convective, shallow convective, and stratiform components. The moist physics parameterization schemes include those for deep convection (ZM95), for shallow convection (Hack 1994) and for stratiform processes (Rasch and Kristjansson 1998 updated by Zhang et al. 2003).

Separate evolution equations have been included for the liquid and ice phase condensate. Condensed water detrained from shallow and frontal convection can form either precipitation or additional stratiform cloud water. Convective precipitation can evaporate into its environment at a rate determined from Sundqvist (1988).

Equations governing cloud condensate include advection and sedimentation of cloud droplets and ice particles. The settling velocities for liquid- and ice-phase constituents are computed separately as functions of particle size characterized by the effective radius. With the increase in size of the ice particles, there is a smooth transition to a different formulation for fall speeds following Locatelli and Hobbs (1974). In the case of liquid drops, fall velocities are calculated using Stokes equation for the entire range of sizes. For further details on the formulation of NCAR CAM3, see Collins et al. (2006).

3 Details of numerical simulations

For this work, we carried out two sets of numerical experiments, one in an aqua-planet framework and the other in an actual-planet framework. It is known from some of the previous studies (Mishra et al. 2008; Mishra and Srinivasan 2010) that an aqua-planet framework is useful in clearly demonstrating the individual effects of the physical parameterizations. For example, Hess et al. (1993) used an aqua-planet framework with simplified SSTs to investigate the sensitivity of model simulations to two different convective parameterization schemes. They reported that there were significant differences in the model-simulated tropical ITCZ, due entirely to the convection schemes. Similar conclusions have been reported by some of the other studies as well (for example, Neale and Hoskins 2000a, b; Mishra and Sahany 2011a, b). In the current aqua-

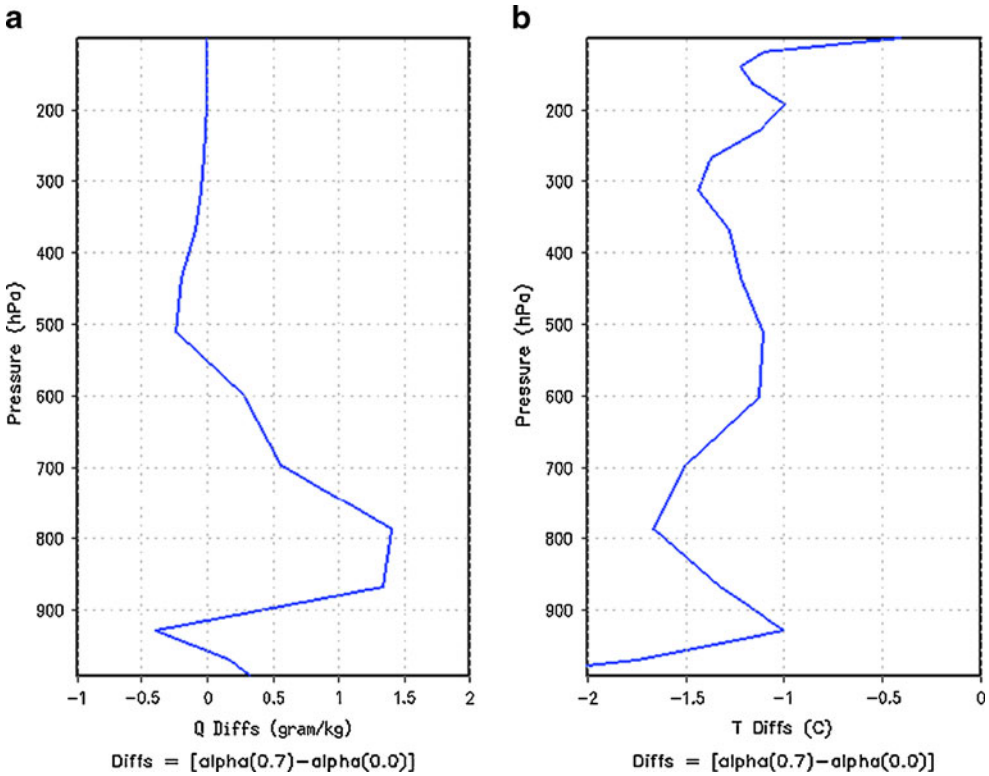

Fig. 5 Vertical structure of the time mean area averaged (0E to 360E and 7S to 7N) quantities for [alpha (0.7)−alpha (0.0)]: **a** Q and **b** T

planet framework, all the experiments have been performed with a zonally symmetric SST profile as boundary condition. The distribution of SST used in the simulation is given in Eq. 1 below (following Neale and Hoskins 2000a, b):

$$T_s(\lambda,\phi) = 27[1-\sin^2(3\phi/2)]^{\circ}\mathrm{C} \quad : -\pi/3 < \phi < \pi/3$$
$$0^{\circ}\mathrm{C} \quad : \text{Otherwise} \tag{1}$$

where T_S=sea surface temperature (°C), λ=longitude, and ϕ=latitude.

The intensity of convective downdrafts was varied by changing the value of the parameter "α" (hereafter referred to as "alpha") shown in the following downdraft formulation (ZM95), with the default value being 0.1:

$$M_d(Z) = ((-\alpha \times M_b) \times (\exp(\lambda_m \times (Z_d - Z)) - 1))/(\lambda_m \times (Z_d - Z)) \tag{2}$$

where M_d is the downdraft mass flux at any height Z, α is the proportionality factor, M_b is the cloud base mass flux, λ_m is the maximum downdraft entrainment rate, and Z_d is the height of initiation of downdrafts. A set of integrations was performed with various values of alpha, ranging from 0 to 1. The initial condition for all simulations was from a previous aqua-planet simulation. All the integrations were

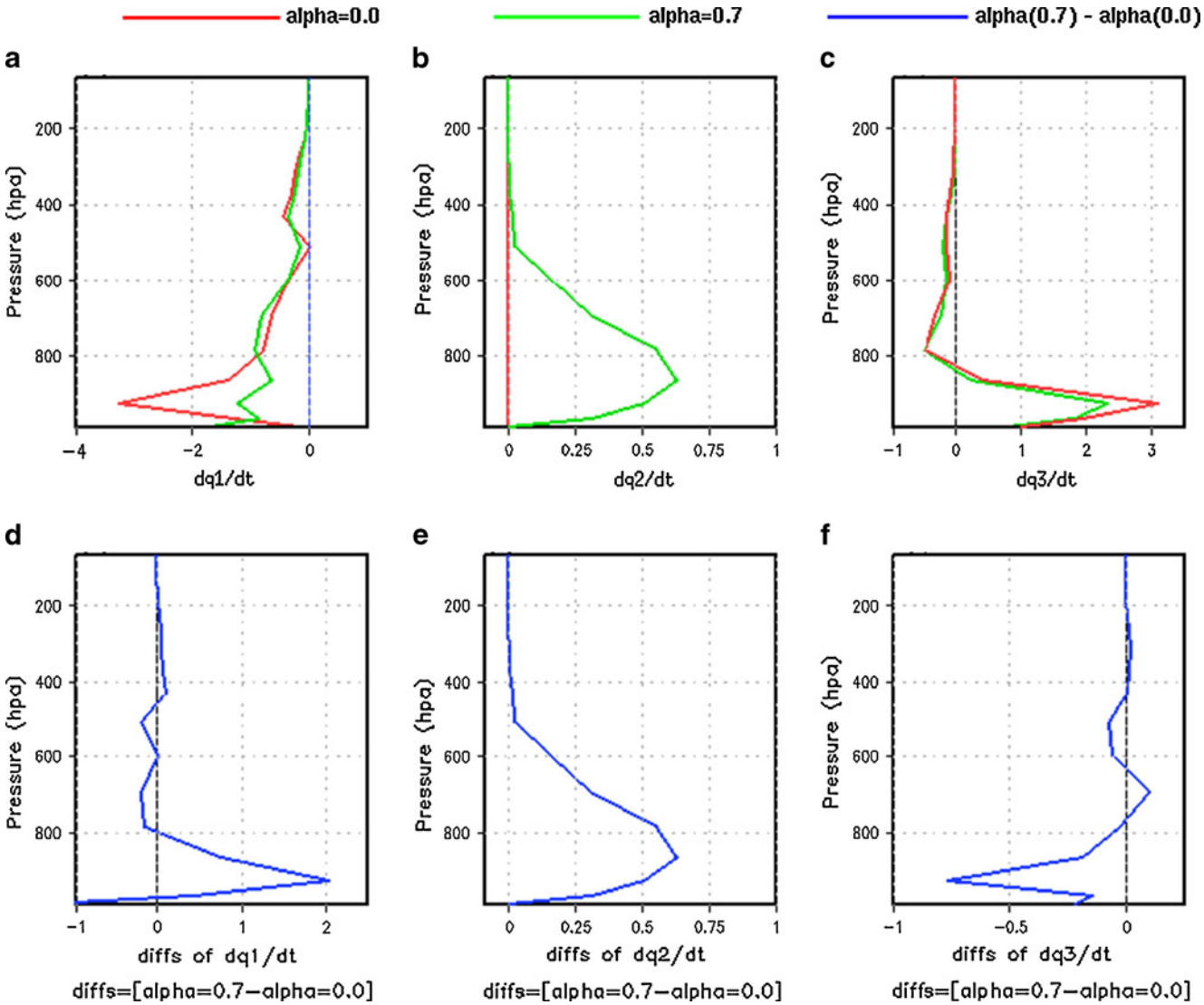

Fig. 6 Vertical profile of the area averaged (0E to 360E and 7S to 7N), time mean quantities. **a** dq_1/dt (specific humidity tendency due to condensation) for alpha=0.0 and alpha=0.7 (kg m^{-2} day^{-1}), **b** dq_2/dt (specific humidity tendency due to evaporation in the downdraft) for alpha=0.0 and alpha=0.7 (kg m^{-2} day^{-1}), **c** dq_3/dt (specific humidity tendency due to lateral moisture advection into the region) for alpha=0.0 and alpha=0.7 (kg m^{-2} day^{-1}), **d** dq_1/dt difference (alpha=0.7−alpha=0.0), **e** dq_2/dt difference (alpha=0.7−alpha=0.0), and **f** dq_3/dt difference (alpha=0.7−alpha=0.0)

performed for 18 months, and the last 12 months of data were used for analysis.

Finally, in order to explore how the aqua-planet results translate to a full AGCM, numerical integrations were performed in an actual-planet framework. All the simulations have been carried out with the semi-Lagrangian dynamical core, with 128×64 horizontal resolution, 26 vertical levels, and a 60-min time step size. It uses realistic land-ocean distribution with topography, observed sea surface temperature and seasonal cycle of solar radiation. Two 10-year (1979–1988) model integrations were carried out with observed SST, one with alpha=0.0 and another with alpha=0.7, owing to the reasons discussed in the following section.

4 Results

We first analyze the zonally averaged time mean value of total rainfall for three different values of alpha, namely, 0.0,

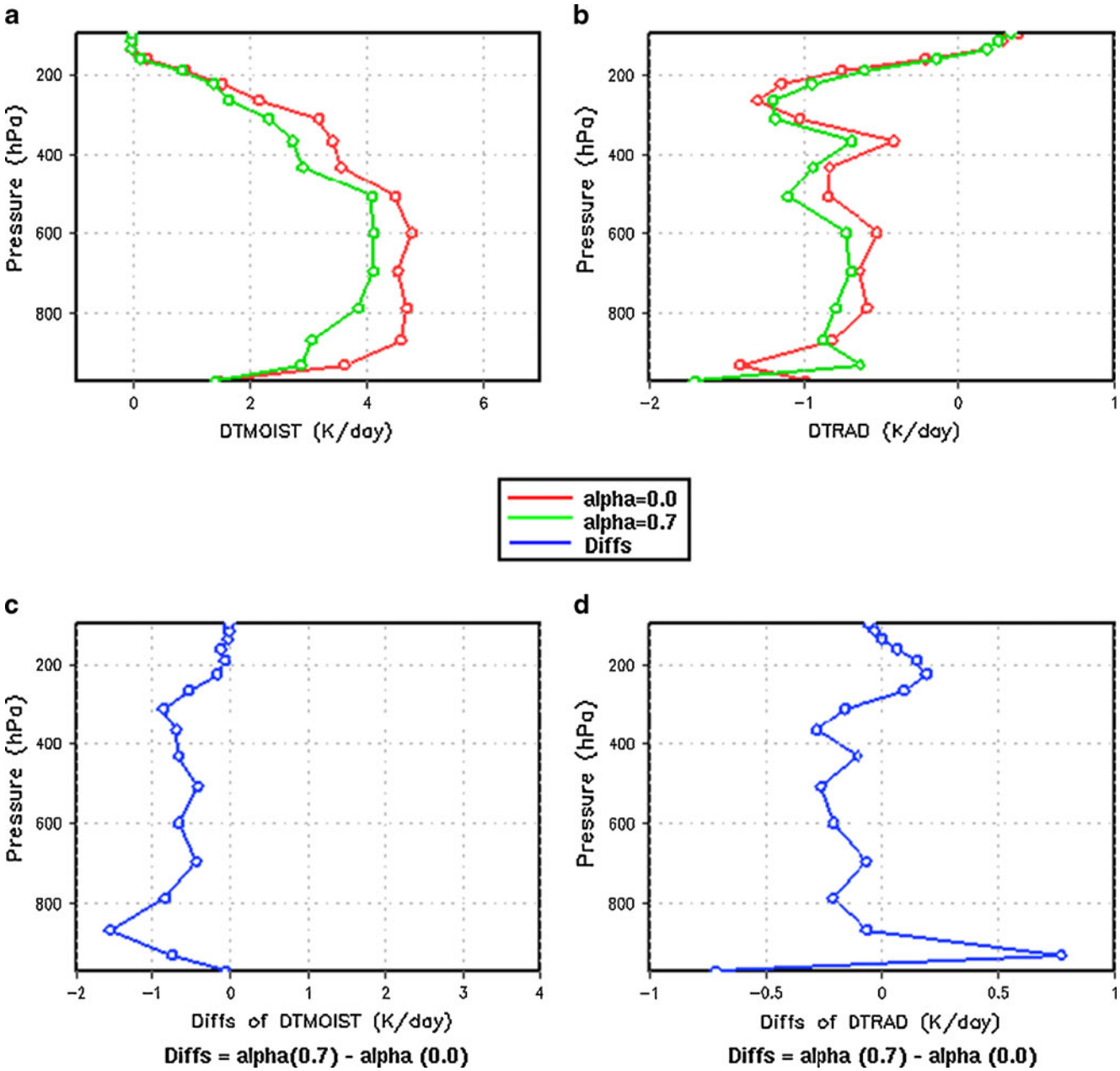

Fig. 7 Top panel shows the vertical structure of the time mean area averaged (0E to 360E and 7S to 7N) quantities for alpha=0.0 and alpha=0.7. **a** Temperature tendency due to moist processes, **b** temperature tendency due to radiative processes, **c**, **d** corresponding differences (alpha=0.7−alpha=0.0), respectively

0.1 (default value), and 1.0 (highest value). It can be seen from Fig. 1 that the maximum impact or sensitivity of model-simulated rainfall to the various downdraft intensities is in the deep tropics (7S–7N). Thus, rest of the analysis in this paper will focus on this zonal belt, for the purpose of clarity.

4.1 Individual components of rainfall

Next, we analyze the impact of downdraft strength on the simulation of each of the rainfall components, namely, deep convective, shallow convective, and stratiform precipitation. Figure 2 shows the area-averaged (0E to 360E and 7S to 7 N) rainfall components for different values of alpha. Interestingly, with the increase of alpha, while there is a reduction in the deep convective rainfall (DRF), there is an increase in the shallow convective rainfall (SRF) and the large-scale rainfall (LRF), as can be seen from Fig. 2a–c. Since the total rainfall (TRF) is primarily governed by the DRF, it seems to vary in a way similar to DRF (see Fig. 2a, d). It can also be seen from the figure that for alpha values >0.7, there is no significant differences in the model-simulated rainfall components. Hence, model simulations with alpha values of 0 and 0.7 are used for further analysis.

4.1.1 Deep convective rainfall

In order to investigate the cause behind the decrease in DRF with increasing alpha, we analyze the area-averaged

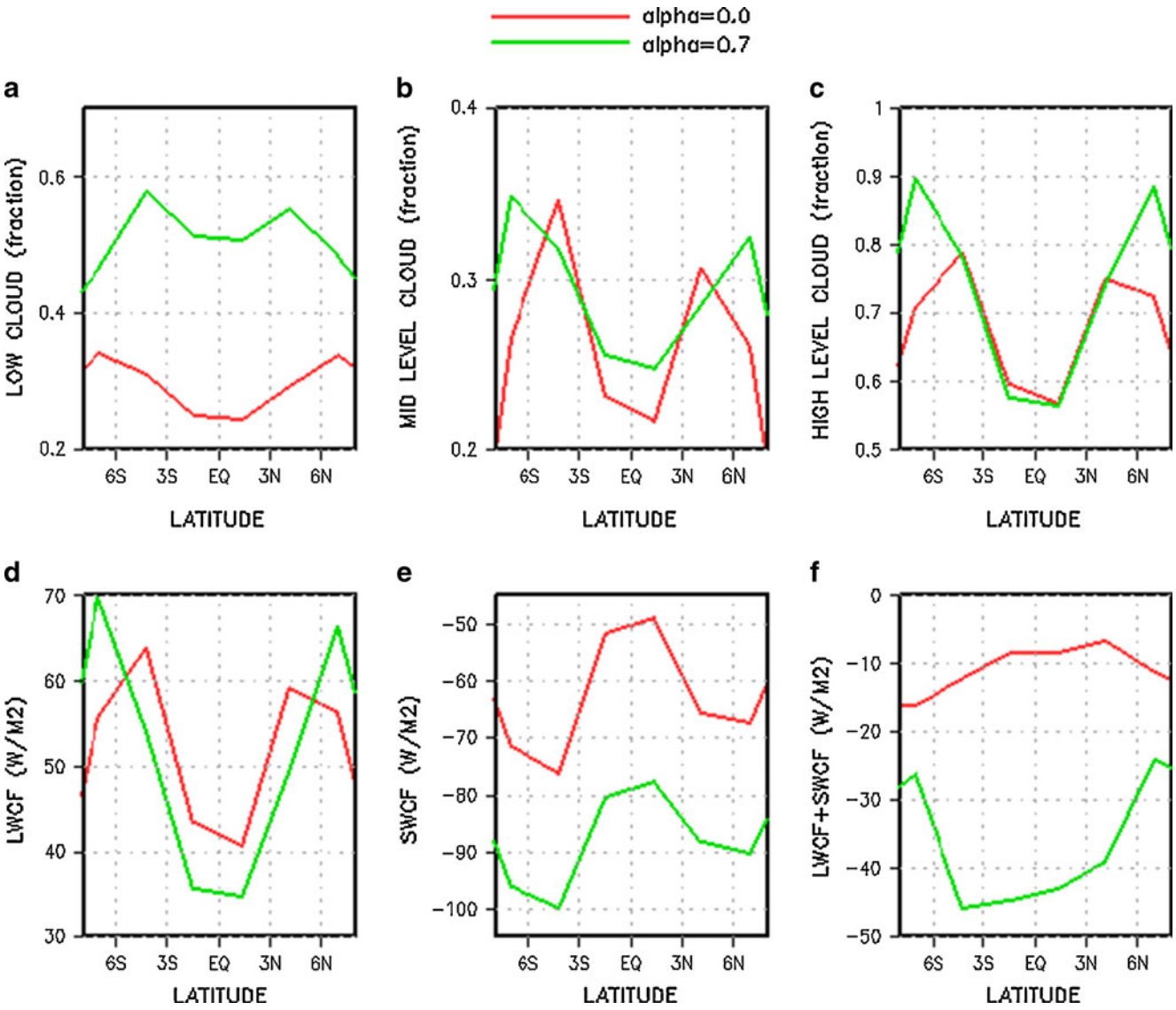

Fig. 8 Zonally averaged time mean quantities for alpha=0 and alpha=0.7. **a** Low cloud (fraction), **b** mid-level cloud (fraction), **c** high level cloud (fraction), **d** longwave cloud radiative forcing (W/m^2), **e** shortwave cloud radiative forcing (W/m^2), and **f** net (long wave+short wave) cloud radiative forcing (W/m^2)

(0E to 360E and 7S to 7 N) vertical profiles of rainfall production and its subsequent evaporation, as can be seen from Fig. 3. Interestingly, there seems to be no significant difference in rainfall production, for the two cases (alpha=0.0 and alpha=0.7), as can be seen from Fig. 3a. Although the same amount of rainfall is produced in the two cases, the amount of precipitation that is evaporated back into the atmosphere is more with alpha=0.7. The amount of falling precipitation that gets evaporated into the atmosphere, essentially consists of two components, namely, sub-grid scale evaporation (to keep the convective downdrafts in a saturated state) and large-scale or grid-scale evaporation (as shown in Fig. 3b, c). While the vertical structure of the sub-grid scale evaporation from the falling precipitation is found to be as expected (see Fig. 3b), the grid-scale evaporation in Fig. 3c shows an intriguing structure. It can be seen from Fig. 3c that with alpha=0.7, the evaporation of falling precipitation into the ambient environment is significantly lower than that with alpha=0.0. This can be explained by the higher relative humidity of the environment (and hence a lower saturation deficit) with alpha=0.7, as can be seen from Fig. 4e.

4.1.2 Shallow convective rainfall and stratiform rainfall

Since it was seen that there is an increase in SRF and LRF with increase in alpha, we further investigate the reasons behind this model behavior. The computation of SRF in the model primarily depends on the moist static energy (MSE) and the cloud water content, while that of LRF depends on RH and water condensate. Hence, we further analyze the vertical structure of these variables and show it in Fig. 4. It can be seen from Fig. 4a–d that the vertical profile of SRF is found to be consistent with that of MSE and cloud water content, while that of LRF can be largely explained by the RH and water condensate profiles (see Fig. 4b, e, f).

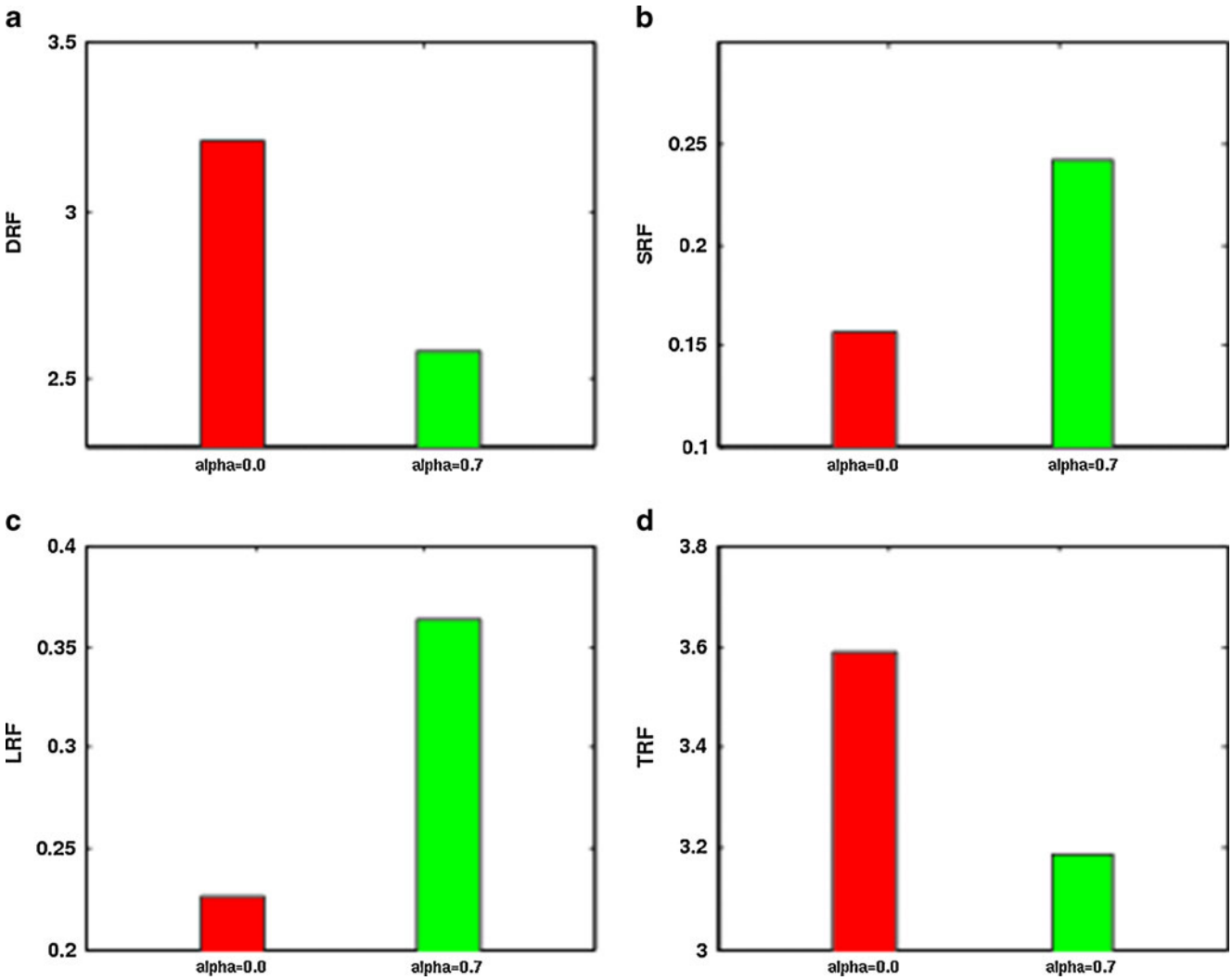

Fig. 9 Area averaged (0E to 360E and 30S to 30N), time mean (all months of 10 years) quantities for alpha=0.0 and alpha=0.7. **a** Deep convective rainfall (mm/day), **b** shallow convective rainfall (mm/day), **c** large-scale rainfall (mm/day), and **d** total rainfall (mm/day)

4.2 Moisture and temperature

Since convective downdrafts can be important in altering the vertical structure of moisture and temperature, we further analyze these variables. Figure 5 shows the difference in vertical structure of specific humidity and temperature for the two model simulations. It can be seen from Fig. 5a that, with strong downdrafts, the boundary layer becomes drier, whereas there is an enhanced moistening of the lower and mid-troposphere. On the other hand, there is no such vertical structure for temperature, and there is a uniform reduction in temperature throughout the atmosphere (see Fig. 5b). The vertical structure of MSE and RH seen from Fig. 4 is largely explained by the profiles of specific humidity and temperature shown in Fig. 5.

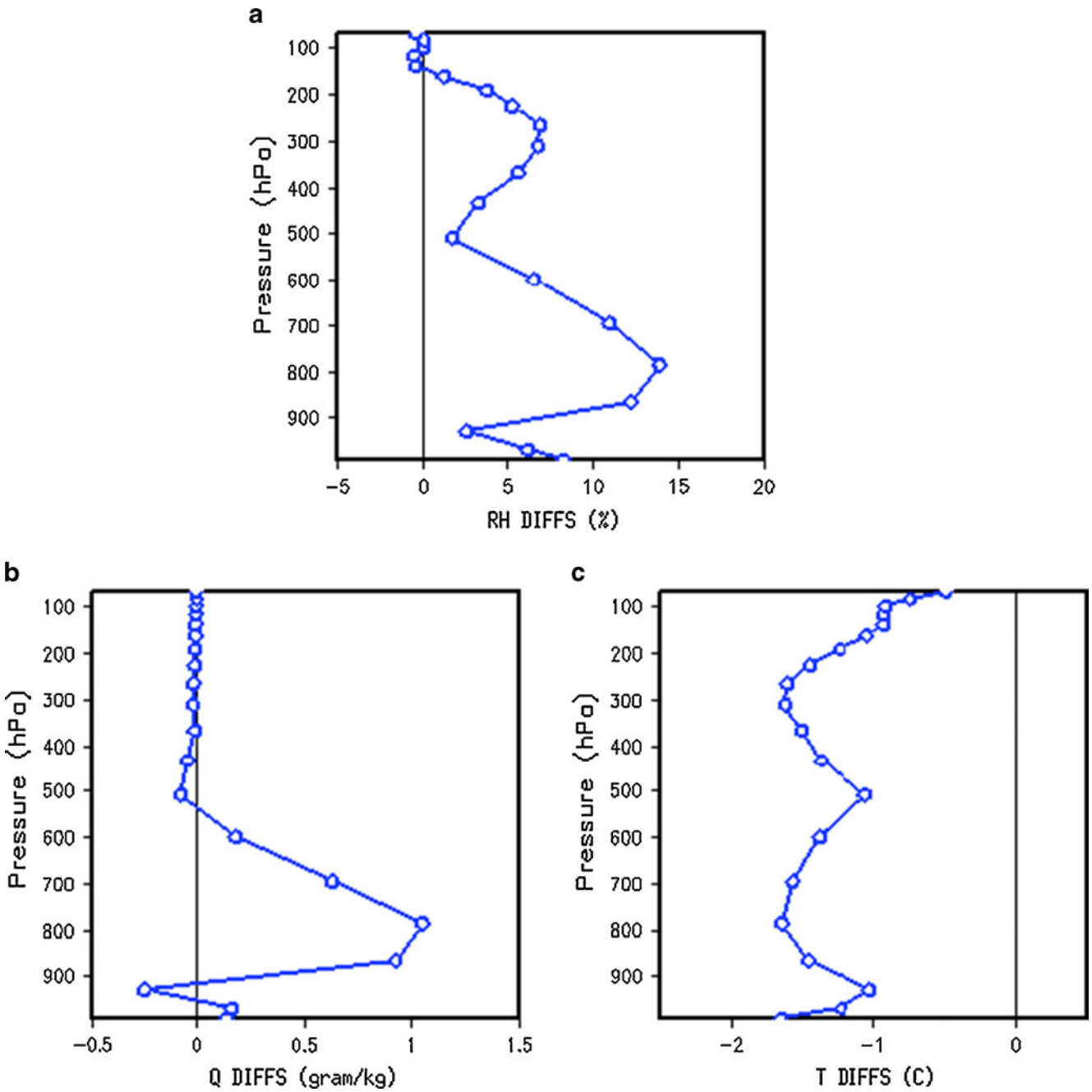

Fig. 10 Vertical profile of the difference (alpha=0.7−alpha=0.0) of the area averaged, time mean quantities for the raining points over the tropics. Grid points where the total rainfall is more than 1 mm/day are considered as the raining points. **a** Relative humidity difference (%), **b** specific humidity difference (g/kg), and **c** atmospheric temperature difference (°C). Time mean is calculated by averaging over all the months of 10 years

In order to explain the vertical structure of specific humidity difference shown in Fig. 5a, we further analyze the specific humidity tendencies due to condensation, evaporation within the downdrafts, and that due to large-scale moisture advection (see Fig. 6). It can be seen from Fig. 6 that the drying of the boundary layer with alpha=0.7, is primarily due to moisture divergence from the region, whereas the moistening of the lower and mid-troposphere is due to the combined effect of condensation and precipitation evaporation within the downdrafts.

In order to explain the vertical structure of the differences in temperature for the two simulations (shown in Fig. 5b), we analyze the vertical profiles of temperature tendencies due to all the moist processes and radiative processes, as shown in Fig. 7. It can be seen from Fig. 7c and d that both moist and radiative processes contribute to the overall reduction in temperature in the atmosphere, with strong downdrafts. Another interesting aspect that can be seen from Fig. 7d is the higher value of temperature tendency due to radiation, around the second model level, with alpha=0.7. To investigate the reason behind the differences in temperature tendencies due to radiative processes, we analyze the low, mid, and high cloud fractions and the corresponding cloud radiative forcing. It can be seen from Fig. 8a that, with strong convective downdrafts, there is a significant increase in the low cloud fraction, throughout the deep tropics (7S-7N), whereas the differences are less pronounced for the mid and high cloud fractions (see Fig. 8b, c). The increase in low cloud fraction with strong downdrafts leads to a corresponding increase in the shortwave cloud forcing and gets translated to the corresponding temperature tendency seen in Fig. 5b.

4.3 Response in actual-planet framework

In order to understand how the impact of convective scale downdrafts in an aqua-planet translates to the real planet framework, numerical simulations were carried out with actual land and sea-ice distribution and fully interactive physics. Observed sea surface temperatures (SSTs) were used as the lower boundary forcing, and the model was integrated for a period of 10 years with alpha values of 0.0 and 0.7.

4.3.1 Area averaged rainfall and its associated quantities

From the aqua-planet simulations, it was seen that with an increase in downdraft intensities, there was a reduction in DRF, while the SRF and LRF were found to increase. In order to verify these findings with the real-planet, we first analyze the area-averaged (0–360, 30S–30N) time mean values for the individual rainfall components. It can be seen from Fig. 9 that the model sensitivity to the downdraft formulation is similar to that seen in the aqua-planet configuration. With alpha=0.7, while there is a reduction in DRF, the SRF and LRF are found to increase (see Fig. 9a–c). In addition, the TRF being largely dominated by DRF shows a similar behavior to that of the latter, as can be seen from Fig. 9a, d.

We next analyze the sensitivity of the model-simulated vertical thermodynamic structure to the downdrafts. It can be seen from Fig. 10 that the results from actual-planet integrations are very similar to those obtained from the aqua-planet simulations. There is an overall increase in RH with the inclusion of downdrafts, which can be seen to

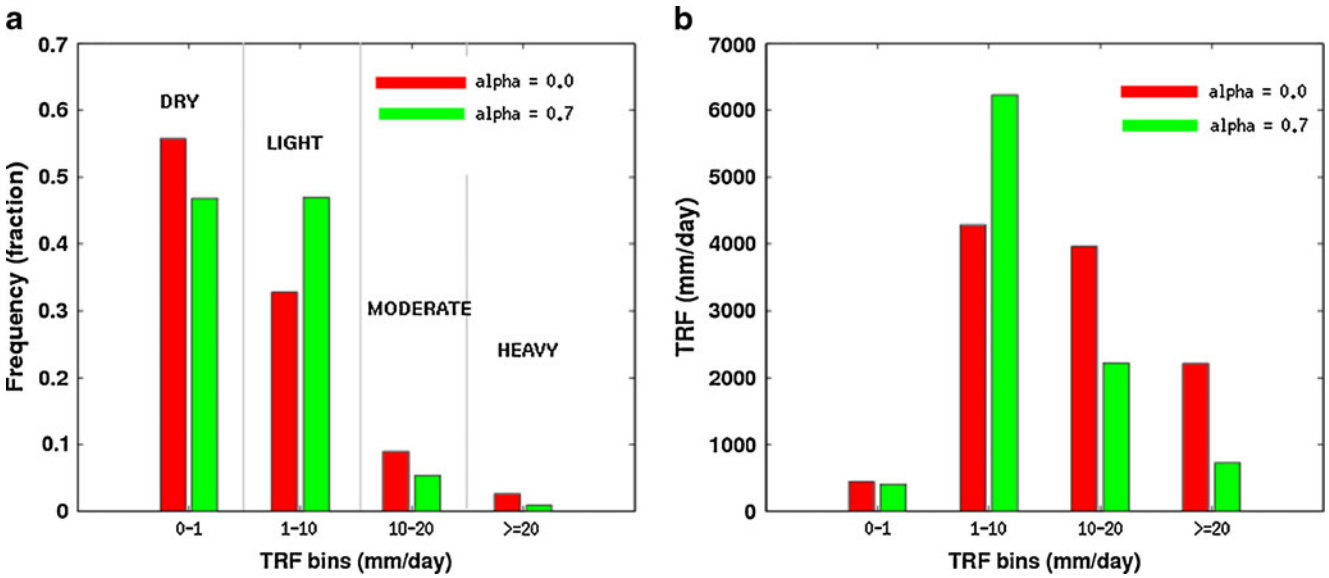

Fig. 11 **a** Frequency distribution of daily precipitation rates in the tropics (0E to 360E and 30S to 30N) for 365 days and **b** amount of precipitation falling into each of the bins

affect the entire troposphere (see Fig. 10a). In the lower and mid-troposphere, the increase in RH can be attributed to the combined effect of moisture and temperature, whereas in the upper troposphere, it is the temperature that largely controls the vertical structure of RH (see Fig. 10a–c).

4.3.2 Frequency and intensity of rainfall

Another important aspect of rainfall is its distribution in terms of frequency and intensity. Hence, we next analyze the impact of convective downdrafts on the model-simulated frequency and intensity of rainfall. Figure 11 shows the frequency distribution of daily precipitation rates and their corresponding accumulations for the two model simulations. It can be seen from Fig. 11 that with alpha= 0.7, excepting the light rainfall bin (1–10 mm/day), there is a reduction in rainfall in all the other bins. The increase in light rain with the inclusion of strong convective downdrafts into the convection scheme seems to be consistent with the higher RH in the atmosphere seen in the preceding figure. In addition, the convection scheme is likely to be triggered more often due to the CAPE-based trigger employed in the ZM scheme (it is to be noted here that SN08 had shown an increase in CAPE with the inclusion of strong convective downdrafts into the ZM scheme).

In order to investigate the role of individual components of TRF in governing its frequency distribution, we further

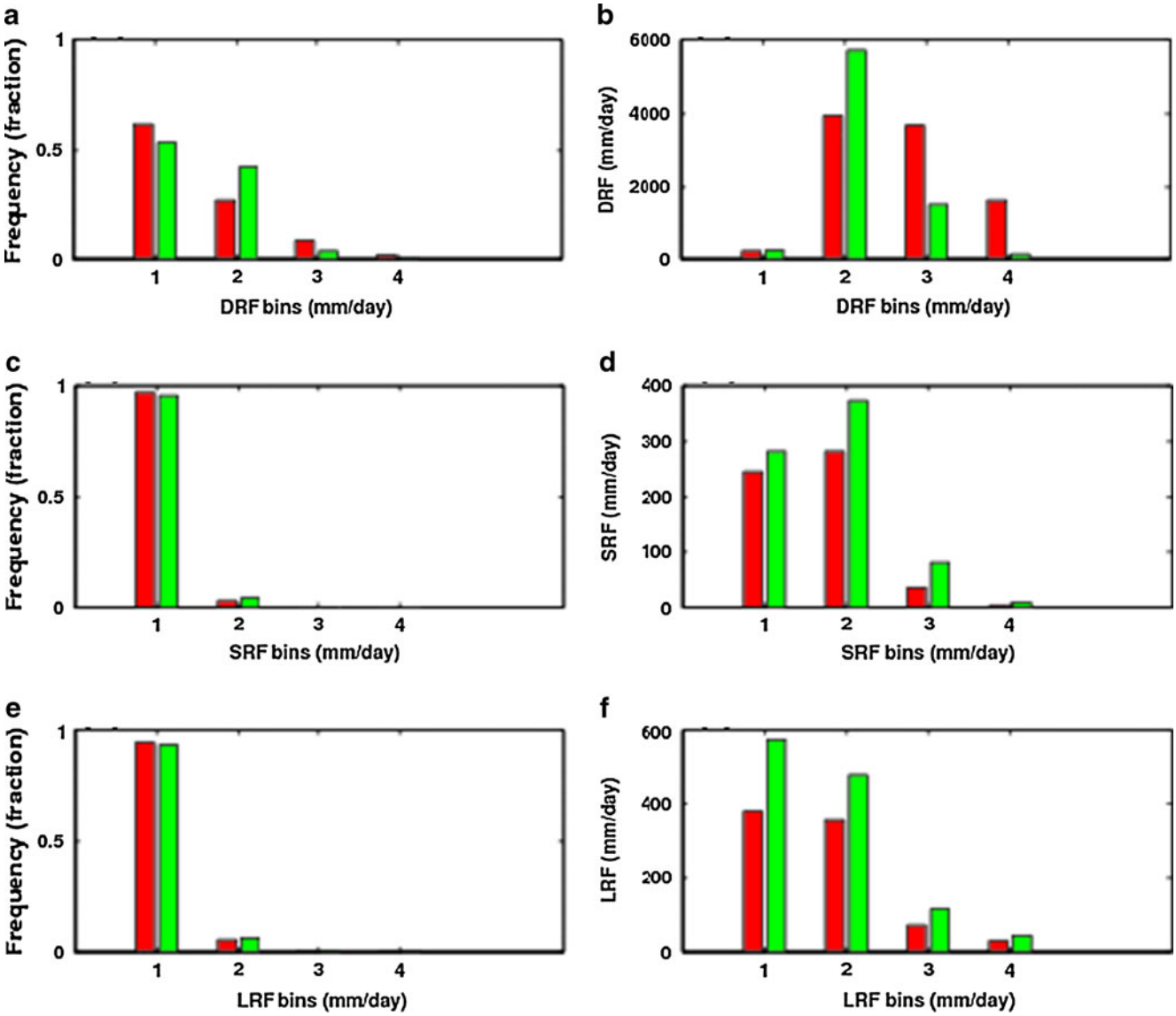

Fig. 12 **a** Frequency distribution of daily deep convective precipitation rates in the tropics (0E to 360E and 30S to 30N) for 365 days, **b** amount of deep convective precipitation falling into each of the bins, **c** as in **a** but for shallow convective precipitation, **d** as in **b** but for shallow convective precipitation, **e** as in **a** but for large-scale precipitation, and **f** as in **b** but for large-scale precipitation

construct similar frequency distribution diagrams for each of them. It can be seen from Fig. 12 that convective downdrafts affect the frequency distribution of each of the rainfall components. It can be seen from Fig. 12c–f that although there are no apparently significant differences in the frequency distribution of rainfall for the chosen bin size, the differences are more pronounced in the total accumulations. This was found to be due to the redistribution of rainfall within the individual bins (figure not shown).

4.3.3 Mean spatial pattern of rainfall

Finally, we analyze the impact of convective downdrafts on the mean spatial pattern of rainfall and contrast it with the corresponding observations. Figure 13 shows the climatological mean (1979–1988) of total rainfall for boreal winter (DJF). It can be seen from the figure that in terms of spatial pattern, both the model simulations agree well with the CMAP observed rainfall. However, as can be seen from Fig. 13d, with alpha=0.7, there is an overall reduction in total rainfall over most parts of the domain. In addition, we also analyze the mean spatial pattern of rainfall during boreal summer, as seen in Fig. 14. It can be seen from the figure that overall there is a good agreement between CMAP and the two model simulations. Interestingly, however, the spatial distribution of rainfall differences is not as homogeneous as was seen in the preceding figure. With inclusion of strong downdrafts into the ZM scheme, while many regions show a decrease in total rainfall, there are a few (see for example western Arabian Sea and the Somali coast) showing a significant increase. Finally, in order to explain the role of each of the rainfall components in shaping the mean spatial pattern of total rainfall, we construct similar plots for the individual components. Figure 15 shows the climatological mean difference in the mean value of the individual rainfall components for the two model simulations, namely, alpha=0.0 and alpha=0.7. It can be seen from Fig. 15 that there is a decrease in DRF and an increase in SRF and LRF with alpha=0.7 (strong convective downdrafts) over most parts of the domain, during both seasons (boreal winter and summer).

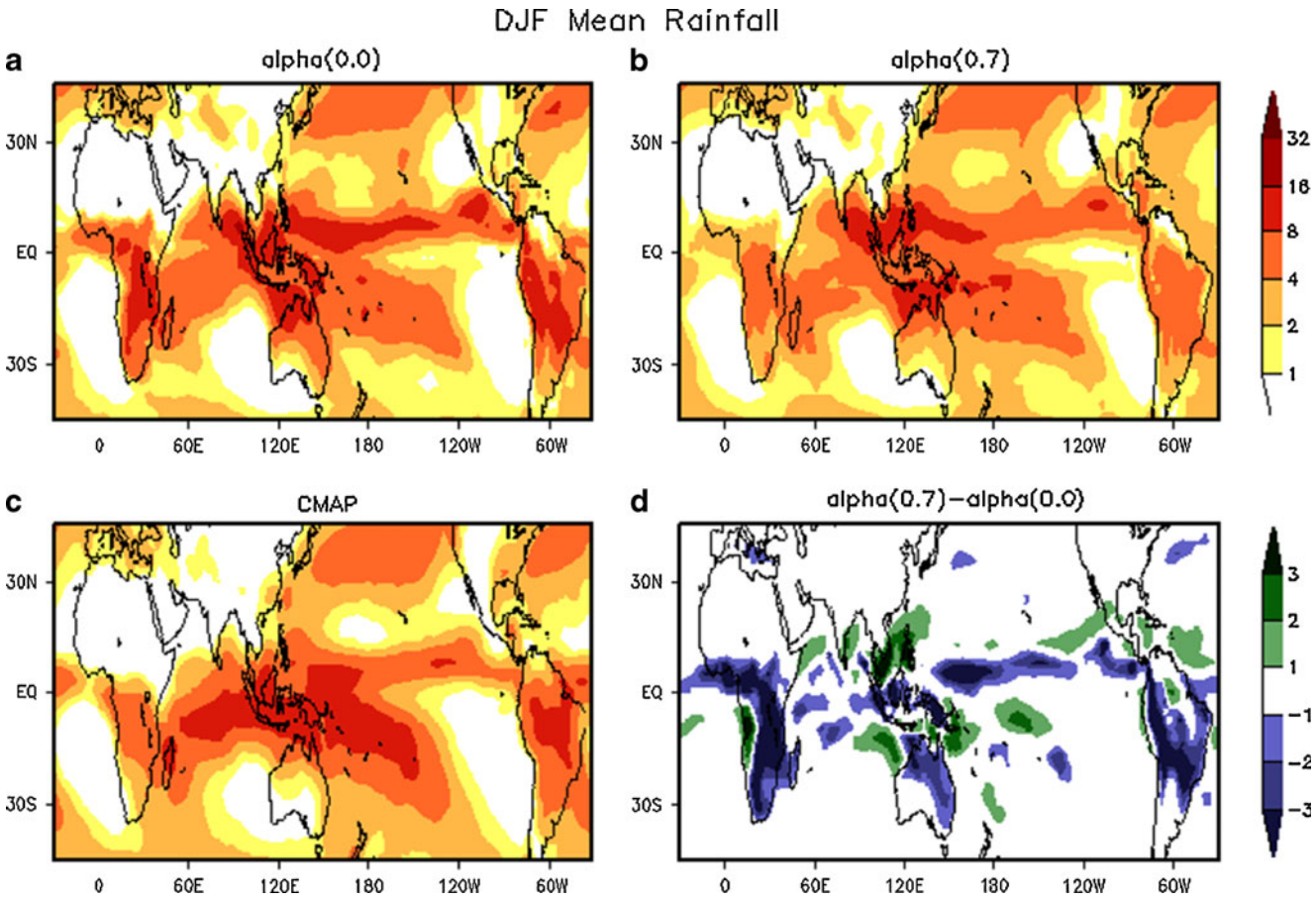

Fig. 13 Climatological mean DJF precipitation (mm/day) for **a** alpha (0.0), **b** alpha(0.7), **c** CMAP, and **d** (alpha=0.7−alpha=0.0). The climatological mean is derived from 10 years (1979–1988) of model output. Pattern correlation has been computed for the region 0E to 360E and 30S to 30N

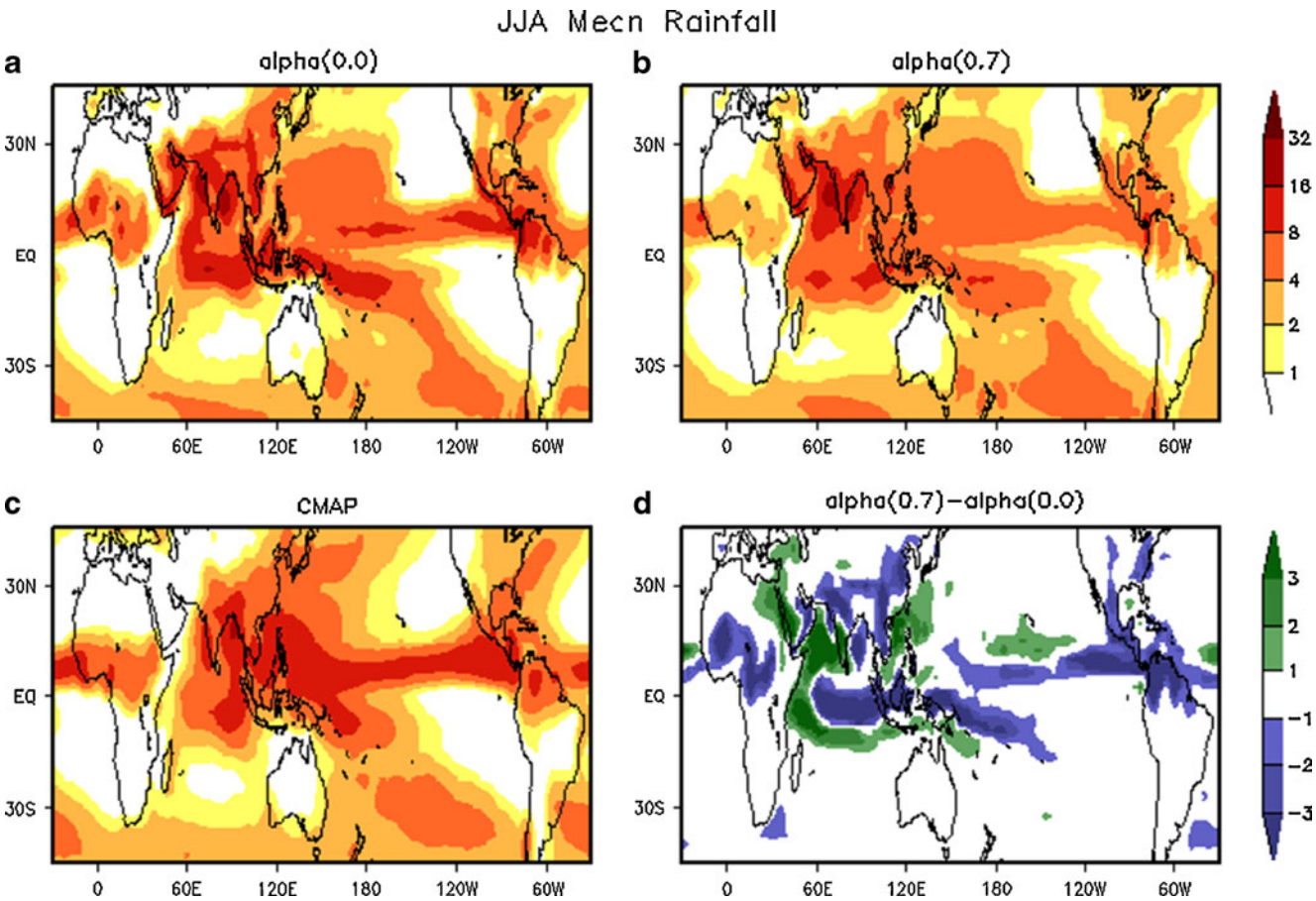

Fig. 14 Same as Fig. 13, but for boreal summer (JJA)

5 Conclusions

This study attempts to make a systematic evaluation of the effect of convective scale downdrafts on the model-simulated rainfall, in both aqua- and actual-planet frameworks, using the NCAR CAM3. It was found that there is a reduction in the total rainfall with stronger downdrafts in the current version of the convective parameterization scheme used in the model. The reduction in total rainfall is primarily attributed to the reduction in the deep convective component (referred to as DRF in the text). With stronger downdrafts, while there is a reduction in DRF, the shallow convective and the large-scale components (referred to as SRF and LRF in the text, respectively) are found to increase. This was confirmed from both aqua- and actual-planet configurations of the model. Interestingly, it is seen that the amount of rainfall production is the same for both cases i.e., the one with no downdrafts and that with strong downdrafts (the two extreme cases used for comparison). However, due to the evaporation of convective precipitation within the downdrafts, there is a reduction in the amount of deep convective precipitation that makes it to the surface. This explains the reduction in DRF with an increase in the intensity of convective downdrafts.

The increase in SRF, with an increase in downdraft intensity was found to be due to the combined effect of the changes in moist static energy of the environment and the cloud water content. Similarly, an increase in LRF with an increase in downdraft intensity was found to be primarily due to the increase in relative humidity (RH) of the environment. This increase in RH was further found to be due to the combined effect of both moisture and temperature. There was an overall increase in specific humidity of the atmosphere with stronger downdrafts, excepting at around 900 hPa. While the overall increase can be attributed to the increase in specific humidity tendency due to condensation and that due to evaporation within the downdrafts, the reduction in specific humidity at around 900 hPa is due to the moisture divergence around this level. In regard to the reduction in temperature throughout the troposphere, it was seen that the primary cause behind this was the reduction in the overall temperature tendency due to moist processes and also that due to the radiative processes. The change in the radiative forcing was further found to be primarily due to a significant increase in the low cloud fraction with strong downdrafts.

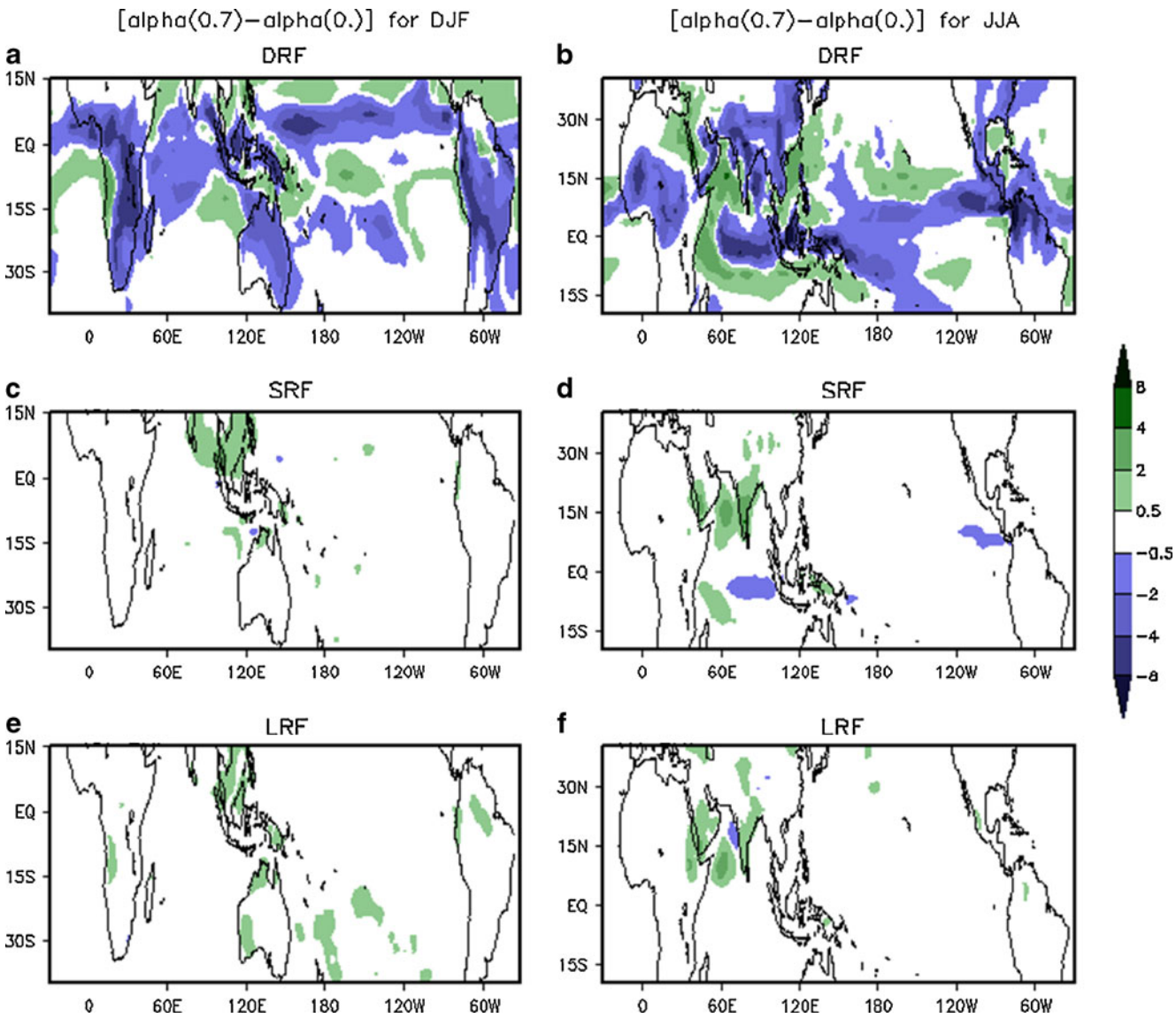

Fig. 15 Difference (alpha=0.7−alpha=0.0) in the climatological mean precipitation (mm/day). The *left panel* is for DJF and the *right panel* for JJA. **a**, **b** Deep convective rainfall, **c**, **d** shallow convective rainfall, and **e**, **f** large-scale rainfall

Results from the actual-planet simulations were found to be very similar to those obtained from the aqua-planet configuration, thus adding credibility to the notion that aqua-planets can be used as a test bed for convective parameterization schemes. Even in the actual-planet framework, it was seen that with strong convective downdrafts there was a reduction in TRF and DRF and an increase in SRF and LRF. The vertical structure of the thermodynamic variables (RH, q, and T) showed similar sensitivity to the downdraft intensity as that seen in the aqua-planet framework.

In addition, the sensitivity of frequency and intensity of model-simulated rainfall to the downdraft intensity was also analyzed, and it was seen that there were significant differences in the frequency distribution of rainfall. It was seen that with an increase in downdraft intensity there is an increase in the frequency of light rain (1–10 mm/day) with a corresponding reduction in all other rainfall bins. A similar behavior was seen for the DRF as well, while the SRF and LRF components showed an increase in rainfall accumulation in all the bins. The increase in frequency of light rain in DRF may be attributed to the increase in CAPE in the atmosphere leading to frequent triggering of the ZM scheme, which uses a CAPE-based trigger function.

Finally, the impact of convective downdrafts on the mean spatial pattern of rainfall was analyzed for the DJF and JJA periods (boreal winter and summer, respectively). For the DJF period, with strong downdrafts, it was seen that, by and large over the whole domain, there was a reduction in DRF and an increase in SRF and LRF. In contrast, during JJA, although a major part of the domain showed a reduction in DRF, there

were regions like western Arabian Sea and the Somali coast with increase in DRF with intense downdrafts. However, the SRF and LRF components showed a spatially homogeneous increase over almost the entire domain.

Thus, from this study, it was seen that the formulation of convective downdrafts in the cumulus parameterization scheme could lead to significant modifications to the model-simulated rainfall and its associated thermodynamic variables. Hence, a more realistic representation of convective downdrafts is essential in the present-day cumulus schemes used in general circulation models used for climate change simulations.

Acknowledgments The authors thankfully acknowledge helpful interactions with David Neelin, Brian Mapes, Mitch Moncrieff, Rich Neale, and Joe Tribbia. Thanks are also due to the anonymous reviewers for helpful comments and suggestions.

References

Collins WD et al (2006) The formulation and atmospheric simulation of the Community Atmosphere Model Version 3 (CAM3). J Clim 19:2144–2161

Hack JJ (1994) Parameterization of moist convection in the National Center for Atmospheric Research Community Climate Model (CCM2). J Geophys Res 99:5551–5568

Hess PG, Battisti DS, Rasch JR (1993) Maintenance of the intertropical convergence zones and the large-scale tropical circulation on a water-covered earth. J Atmos Sci 50:691–713

Locatelli JD, Hobbs PV (1974) Fall speeds and masses of solid precipitation particles. J Geophys Res 79:2185–2197

Mishra SK, Srinivasan J, Nanjundiah RS (2008) The impact of time step on the intensity of ITCZ in aquaplanet GCM. Monthly Weather Review 136:4077–4091

Mishra SK, Srinivasan J (2010) Sensitivity of the simulated precipitation to changes in convective relaxation time scale. Ann Geophys 28:1827–1846

Mishra SK, Sahany S (2011a) Effects of time step size on the simulation of tropical climate in NCAR-CAM3. Clim Dyn 37:689–704. doi:10.1007/s00382-011-0994-4

Mishra SK, Sahany S (2011b) Sensitivity of Kelvin waves and Madden–Julian oscillation to convective downdrafts in the NCAR-CAM3. Atmos Sci Lett 12:281–287. doi:10.1002/asl.334

Molinari J, Corsetti T (1985) Incorporation of cloud scale and mesoscale downdrafts into a cumulus parameterization: results of one- and three-dimensional integrations. Mon Wea Rev 113:485–501

Neale RB, Hoskins BJ (2000a) A standard test for AGCMs including their physical parameterizations. I: the proposal. Atmos Sci Lett 1:101–107

Neale RB, Hoskins BJ (2000b) A standard test for AGCMs including their physical parametrizations. II: results for the Met. Office Model. Atmos Sci Lett 1:156–169. doi:10.1006/asle.2000.0020

Rasch PJ, Kristjansson JE (1998) A comparison of the CCM3 model climate using diagnosed and predicted condensate parameterizations. J Clim 11:1587–1613

Sahany S, Nanjundiah RS (2008) Impact of convective downdrafts on model simulations: results from aqua-planet integrations. Ann Geophys 26:1877–1887

Sundqvist H (1988) Parameterization of condensation and associated clouds in models for weather prediction and general circulation simulation. In: Schlesinger ME (ed) Physically-based modeling and simulation of climate and climate change, vol 1. Kluwer Academic, Dordrecht, pp 433–461

Zhang GJ, McFarlane NA (1995) Sensitivity of climate simulations to the parameterization of cumulus convection in the CCGCM. Atmos Ocean 33:407–446

Zhang M, Lin W, Bretherton CS, Hack JJ, Rasch PJ (2003) A modified formulation of fractional stratiform condensation rate in the NCAR community atmospheric model CAM2. J Geophys Res 108(D1):4035. doi:10.1029/2002JD002523